Speckle statistics of cortical brain tissue in optical coherence tomography

Gary R. Ge[a], Wei Song[b], Maiken Nedergaard[b], Jannick P. Rolland[a,c], and Kevin J. Parker[c,d]

[a]The Institute of Optics, University of Rochester, Rochester, New York, USA
[b]Center for Translational Neuromedicine, University of Rochester Medical Center, Rochester, New York, USA
[c]Department of Biomedical Engineering, University of Rochester, Rochester, New York, USA
[d]Department of Electrical and Computer Engineering, University of Rochester, Rochester, New York, USA

ABSTRACT

A recent theoretical framework using power-law functions was proposed to model scattering from biological tissues in ultrasound and optical coherence tomography. Multi-scale scattering sites such as the fractal branching vasculature will then contribute to power-law based probability distributions of speckle statistics. These distributions are the Burr type XII distribution, the Lomax distribution, and the generalized logistic distribution for speckle amplitude, intensity, and log amplitude, respectively. Previous experiments with ultrasound and optical coherence tomography demonstrate that these distributions are better fits to image histogram data of various biological tissues when compared with classical models (e.g., Rayleigh, K, and gamma distributions). Of critical importance is that this framework provides novel parameters, most notably the power-law exponent parameter, for characterizing the physics of scattering from soft tissue. The typical range for the exponent parameter in other normal tissues is approximately 3 to 6. The aim is for this parameter to be used as a new biomarker for diagnostic imaging, sensitive to changes in tissue structures. Here, we demonstrate a specific application to mouse brain tissue, in which the exponent parameter is used to characterize mouse cortical brain under various conditions including *ex vivo* and *in vivo* using optical coherence tomography.

Keywords: Optical coherence tomography, backscattering, speckle, probability and statistics, power law, fractal, statistical optics, tissue characterization, brain

1. INTRODUCTION

Speckle, the granular texture seen in images generated by interfering waves, and its amplitude statistics have been studied with numerous probability distribution functions (PDFs).[1–10] Classically, these include the Rayleigh and the K distributions, among others.[11–23] Recently, Parker *et al.* provided a new view of tissue scattering, i.e., multi-scale scattering sites such as fractal branching blood vessels lead to a power law distribution of scatterers, and they derived that the resulting speckle statistics would thus follow power-law based distributions.[24–28] The power-law based PDFs are the Burr type XII distribution for speckle amplitude, the Lomax distribution for speckle intensity, and the generalized logistic distribution for the log of amplitude, all of which have two parameters (a power-law exponent parameter and a scaling parameter).[28]

Since then, it has been shown that these new distributions provide good fits to the speckle statistics seen in ultrasound and optical coherence tomography (OCT) scans.[28–30] In particular for OCT, Ge *et al.* showed that these newly proposed PDFs not only fit better to the speckle statistics of various tissue scans (skin, brain, liver, etc.) when compared with the Rayleigh and K PDFs, and also showed that the new PDFs provided a power-law or exponent parameter that can potentially characterize the sample tissue.[29] The resulting estimated power-law

Further author information: (Send correspondence to G.R.G.)
G.R.G.: E-mail: gge@ur.rochester.edu,
K.J.P.: E-mail: kevin.parker@rochester.edu

Biomedical Applications of Light Scattering XII, edited by Adam Wax, Vadim Backman,
Proc. of SPIE Vol. 11974, 1197403 · © 2022 SPIE · 1605-7422 · doi: 10.1117/12.2608850

parameter ranged from approximately 3 to 6, which is within the expected range from theory and numerical simulations. Subsequently, Niemczyk *et al.* confirmed that the Burr distribution offered the best goodness-of-fit among other one- and two-parameter distributions analyzed in their study.[30] In addition, they found that out of multiple parametric PDFs tested, the Burr distribution offered the highest correlation between its parameters and the intraocular pressure (IOP) of *in vivo* human corneas scanned with OCT.

In this manuscript, we utilize this novel framework to further demonstrate that it may be used to characterize mouse cortical brain tissue scanned with OCT in various conditions including *ex vivo*, *in vivo*, and with and without dura mater after cranial window surgery. While more samples and studies are needed to confirm pre-existing results, this study further supports the potential of the power-law based parameters in characterizing tissue. Finally, the importance of investigations regarding exactly which multi-scale structures would lead to power-law based speckle statistics are discussed.

2. RELEVANT EQUATIONS

In this study, we will focus on speckle amplitude statistics of OCT scans. Thus, the two PDFs that will be used for fitting speckle amplitude include the Burr type XII distribution and the Rayleigh distribution. The specific two-parameter Burr distribution is given by

$$p(A;d,b) = \frac{2A(b-1)}{d^2\left[\left(\frac{A}{d}\right)^2+1\right]^b} \tag{1}$$

where A is the amplitude, d is a scale factor, and b is the power-law or exponent parameter. In ultrasound, optics, and radar literature, it is conventional to normalize A by dividing by the root mean square (i.e., replace A with $A/\sqrt{\langle A\rangle^2}$ in Eq. 1).[22]

The Rayleigh PDF is given by

$$p(A) = \frac{2A}{\sqrt{\langle A\rangle^2}}\exp\left(-\frac{A^2}{\langle A\rangle^2}\right) \tag{2}$$

3. METHODS

3.1 Tissue samples

Two wild-type (C57BL6) mice underwent a craniotomy where a 5 mm diameter region of skull was replaced with a special glass window to allow for OCT imaging. This surgery was performed under an acute procedure protocol. Agarose gel was applied under and around the glass window. A custom mount was used to hold the mouse in a stable position for imaging during both *in vivo* and *ex vivo* studies. The dura mater was left intact for the first mouse and removed for the second mouse. For the second mouse, the cranial window was installed on the right hemisphere to avoid excessive bleeding. *Ex vivo* scans were acquired post euthanasia via anesthesia overdose. All mouse studies were performed in accordance with protocols approved by the University of Rochester Committee on Animal Resources.

3.2 Experimental setup

A custom-built phase-sensitive swept-source OCT system was used to obtain 2D B-mode scans. The system was implemented with a swept-source laser (HSL-2100-HW, Santec, Aichi, Japan) with a center wavelength of 1310 nm and a bandwidth of 140 nm. The lateral resolution was approximately 20 µm, and the axial resolution was approximately 6 µm in air. The maximum sensitivity of the system was approximately 110 dB. The imaging depth was 5 mm in air. The OCT system was controlled with LabVIEW (Version 14, National Instruments, Austin, Texas, USA). Single frames with 1000 A-lines were obtained. Regions of interest (ROIs) were selected and speckle amplitude histograms were generated from these regions.

3.3 Data processing and analysis

ROIs were selected for uniform average intensity with avoidance of shadows and other artifacts in the OCT scans of mouse brain. The speckle amplitude histograms were fitted to the Burr distribution using maximum likelihood estimation (MLE) in addition to the Rayleigh distribution. The estimated Burr parameter $\hat{b}$ is the power-law or exponent parameter of interest. Detailed data and image processing is further described in a previous publication.[29] The estimated $\hat{b}$ is then used to compare scans of the brain under different conditions.

4. RESULTS

Figs. 1 and 2 demonstrate OCT scans of the mouse "A" with the associated speckle analysis. ROIs are highlighted in green and both Burr and Rayleigh PDFs are plotted. The estimated Burr power-law parameter $\hat{b}$ is reported along with the 95% confidence interval, as given by the MLE method. Figs. 3 and 4 demonstrate OCT scans of mouse "B" brain with dura mater removed. For both sets of scans, *ex vivo* scans were taken immediately post euthanasia.

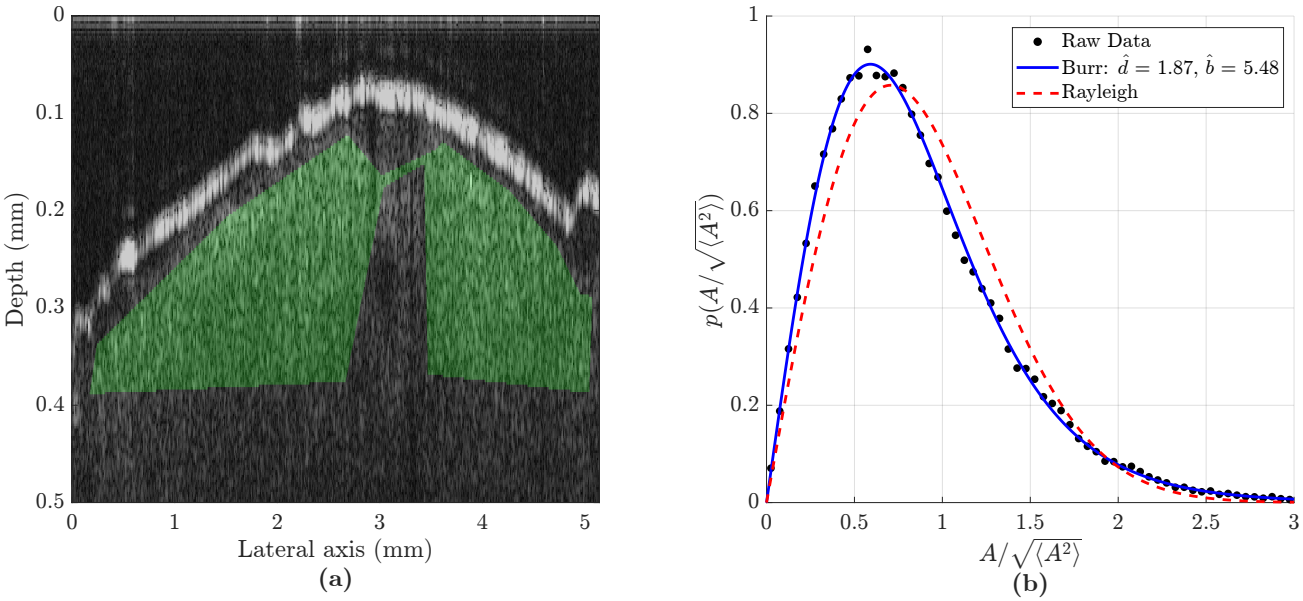

Figure 1. *In vivo* mouse "A" brain OCT scan with dura mater preserved. Cranial window was placed centrally, occupying both hemispheres. (a) 2D B-mode image with ROI highlighted in green. (b) Burr and Rayleigh PDFs fitted to the raw speckle amplitude data. The 95% confidence interval for $\hat{b}$ is [5.28,6.29].

5. CONCLUSION AND DISCUSSION

From Figs. 1 and 2, while there is a small increase in the estimated power-law parameter $\hat{b}$ when the mouse is euthanized, the effect is not significant due to overlap of the confidence intervals. However, when the dura mater is removed, as shown in Figs. 3 and 4, this increase becomes significant. While there is currently not enough data to ascertain the exact mechanism for this increase, we offer a speculative hypothesis. Post euthanasia, the mouse brain is no longer regulated physiologically, and cell death will cause leakage of cerebrospinal fluid throughout the brain.[31] Cerebral edema and swelling may follow, which further augments this process. Thus, the multi-scale scatterers in the brain shift from power-law based distributions to that producing Rayleigh statistics. As the power-law parameter $\hat{b}$ increases, the Burr distribution converges to the Rayleigh distribution. When the protective dura mater is removed, the post-mortem effect is even more significant since the initial *in vivo* scans can be considered baseline scans. Without the dura mater, the brain is more susceptible to physiological dysregulation. However, this would also suggest that the two mice had different baselines for the power-law parameter. More samples would be needed to confirm these trends. Future studies are necessary to confirm these results and to determine the sensitivity of the Burr parameter $\hat{b}$ to subtle changes in brain structures during aging and the onset of diseases.

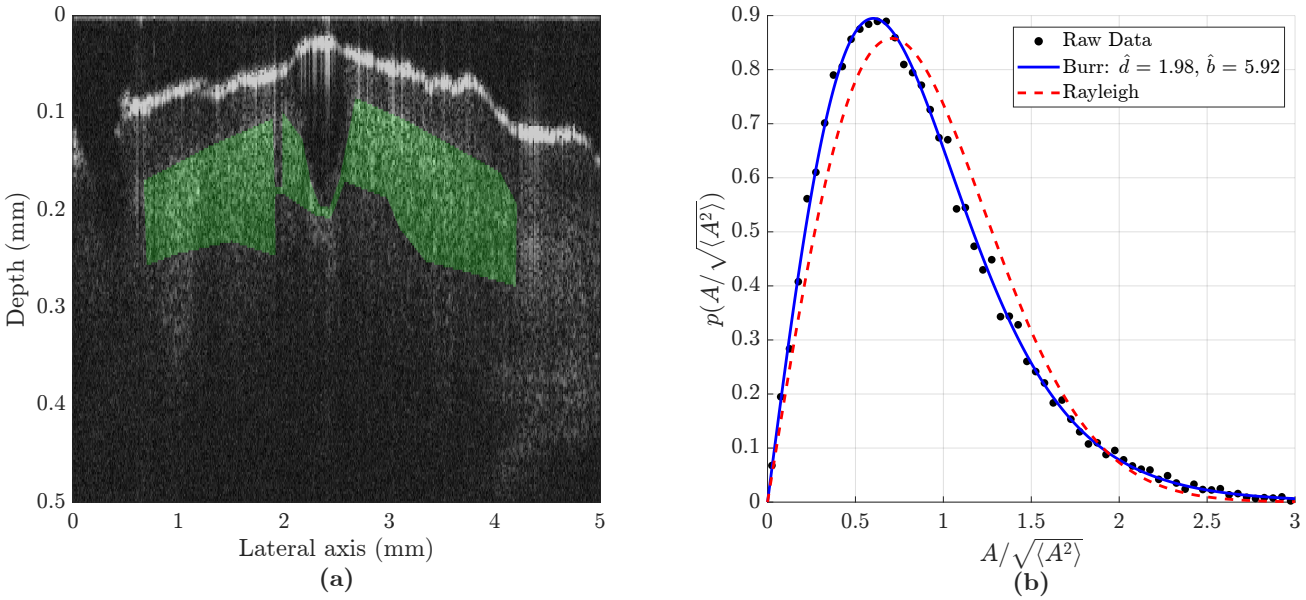

Figure 2. *Ex vivo* mouse brain "A" OCT scan with dura mater preserved (same mouse as in Fig. 1, post euthanasia). Cranial window was placed centrally, occupying both hemispheres. (a) 2D B-mode image with ROI highlighted in green. (b) Burr and Rayleigh PDFs fitted to the raw speckle amplitude data. The 95% confidence interval for $\hat{b}$ is [5.57,6.28].

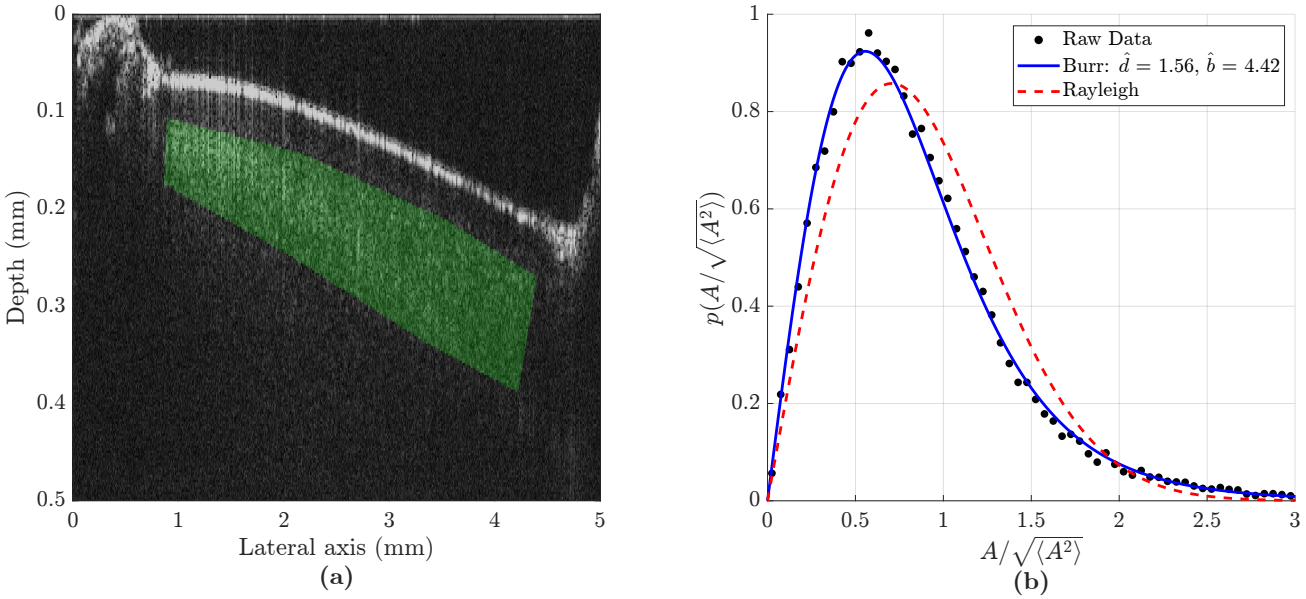

Figure 3. *In vivo* mouse "B" brain OCT scan with dura mater removed. Cranial window was placed on the right hemisphere. (a) 2D B-mode image with ROI highlighted in green. (b) Burr and Rayleigh PDFs fitted to the raw speckle amplitude data. The 95% confidence interval for $\hat{b}$ is [4.26,4.58].

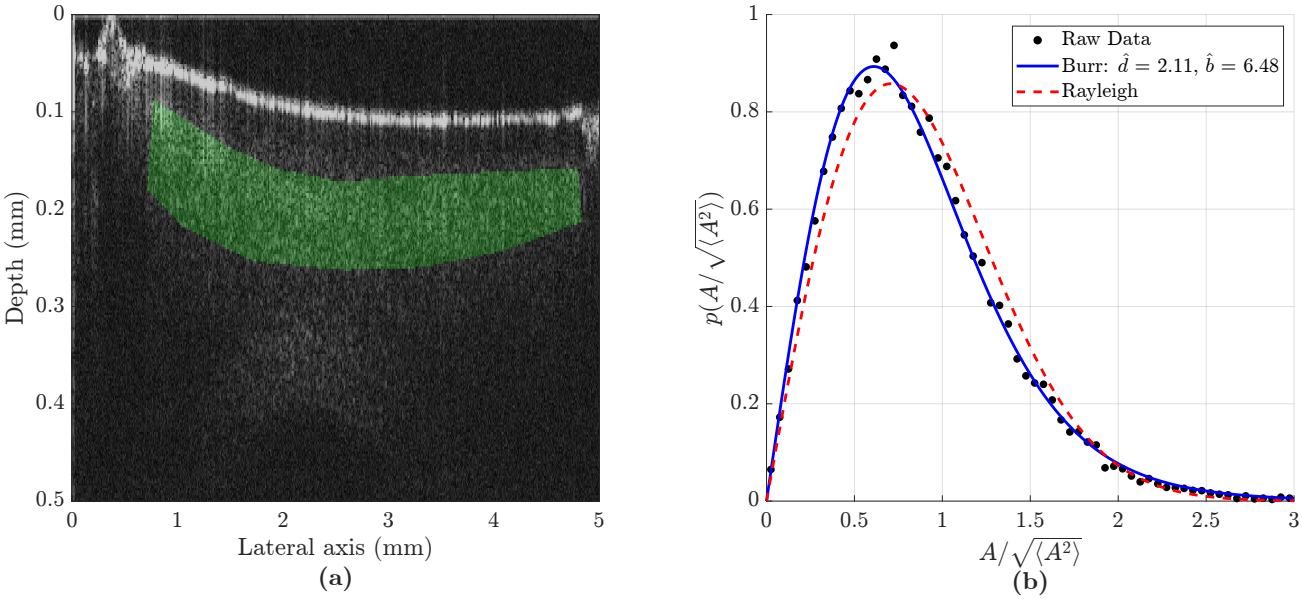

Figure 4. *Ex vivo* mouse "B" brain OCT scan with dura mater removed (same mouse as in Fig. 3, post euthanasia). Cranial window was placed on the right hemisphere. (a) 2D B-mode image with ROI highlighted in green. (b) Burr and Rayleigh PDFs fitted to the raw speckle amplitude data. The 95% confidence interval for $\hat{b}$ is [6.10,6.86].

ACKNOWLEDGMENTS

Gary Ge is supported by the National Institutes of Health under award number F30AG069293. The work is also supported by NIH grants R21EB025290 and R21AG070331. The content is solely the responsibility of the authors and does not necessarily represent the official views of the National Institutes of Health.

REFERENCES

[1] Goodman, J. W., [*Statistical properties of laser speckle patterns*], vol. 9 of *Topics in Applied Physics*, 9–75, Springer-Verlag, Heidelberg (1975).

[2] Goodman, J. W., "Some fundamental properties of speckle," *J Opt Soc Am* **66**(11), 1145–1150 (1976).

[3] Dainty, J. C., [*I The Statistics of Speckle Patterns*], vol. 14, 1–46, Elsevier (1977).

[4] Burckhardt, C. B., "Speckle in ultrasound B-mode scans," *IEEE Trans Sonics Ultrason* **25**(1), 1–6 (1978).

[5] Wagner, R. F., Smith, S. W., Sandrik, J. M., and Lopez, H., "Statistics of speckle in ultrasound B-scans," *IEEE Transactions on Sonics and Ultrasonics* **30**(3), 156–163 (1983).

[6] Oosterveld, B. J., Thijssen, J. M., and Verhoef, W. A., "Texture of B-mode echograms: 3-D simulations and experiments of the effects of diffraction and scatterer density," *Ultrason Imaging* **7**(2), 142–60 (1985).

[7] Bashkansky, M. and Reintjes, J., "Statistics and reduction of speckle in optical coherence tomography," *Optics Letters* **25**(8), 545–547 (2000).

[8] Thijssen, J. M., "Ultrasonic speckle formation, analysis and processing applied to tissue characterization," *Pattern Recogn Lett* **24**(4), 659–675 (2003).

[9] Karamata, B., Hassler, K., Laubscher, M., and Lasser, T., "Speckle statistics in optical coherence tomography," *Journal of the Optical Society of America A* **22**(4), 593–596 (2005).

[10] Lindenmaier, A. A., Conroy, L., Farhat, G., DaCosta, R. S., Flueraru, C., and Vitkin, I. A., "Texture analysis of optical coherence tomography speckle for characterizing biological tissues in vivo," *Optics Letters* **38**(8), 1280–1282 (2013).

[11] Rayleigh, L., "XII. On the resultant of a large number of vibrations of the same pitch and of arbitrary phase," *The London, Edinburgh, and Dublin Philosophical Magazine and Journal of Science* **10**(60), 73–78 (1880).

[12] Jakeman, E. and Tough, R. J. A., "Generalized K distribution: a statistical model for weak scattering," *J Opt Soc Am A* **4**(9), 1764–1772 (1987).
[13] Tuthill, T. A., Sperry, R. H., and Parker, K. J., "Deviations from Rayleigh statistics in ultrasonic speckle," *Ultrason Imaging* **10**(2), 81–9 (1988).
[14] Cramblitt, R. M. and Parker, K. J., "Generation of non-Rayleigh speckle distributions using marked regularity models," *IEEE Trans Ultrason Ferroelectr Freq Control* **46**(4), 867–874 (1999).
[15] Prager, R. W., Gee, A. H., Treece, G. M., and Berman, L. H., "Analysis of speckle in ultrasound images using fractional order statistics and the homodyned K-distribution," *Ultrasonics* **40**(1-8), 133–7 (2002).
[16] Shankar, P. M., "A compound scattering PDF for the ultrasonic echo envelope and its relationship to K and Nakagami distributions," *IEEE Trans Ultrason Ferroelectr Freq Control* **50**(3), 339–43 (2003).
[17] Destrempes, F. and Cloutier, G., "A critical review and uniformized representation of statistical distributions modeling the ultrasound echo envelope," *Ultrasound Med Biol* **36**(7), 1037–51 (2010).
[18] Zaitsev, V. Y., Matveev, L. A., Matveyev, A. L., Gelikonov, G. V., and Gelikonov, V. M., "A model for simulating speckle-pattern evolution based on close to reality procedures used in spectral-domain OCT," *Laser Physics Letters* **11**(10), 105601 (2014).
[19] Kirillin, M. Y., Farhat, G., Sergeeva, E. A., Kolios, M. C., and Vitkin, A., "Speckle statistics in OCT images: Monte carlo simulations and experimental studies," *Optics Letters* **39**(12), 3472–3475 (2014).
[20] Weatherbee, A., Sugita, M., Bizheva, K., Popov, I., and Vitkin, A., "Probability density function formalism for optical coherence tomography signal analysis: a controlled phantom study," *Optics Letters* **41**(12), 2727–2730 (2016).
[21] Almasian, M., van Leeuwen, T. G., and Faber, D. J., "OCT amplitude and speckle statistics of discrete random media," *Scientific Reports* **7**(1), 14873 (2017).
[22] Stanton, T. K., Lee, W., and Baik, K., "Echo statistics associated with discrete scatterers: A tutorial on physics-based methods," *J Acoust Soc Am* **144**(6), 3124–3171 (2018).
[23] Tsai, Y. W., Zhou, Z., Gong, C. A., Tai, D. I., Cristea, A., Lin, Y. C., Tang, Y. C., and Tsui, P. H., "Ultrasound detection of liver fibrosis in individuals with hepatic steatosis using the homodyned K distribution," *Ultrasound Med Biol* **47**(1), 84–94 (2021).
[24] Parker, K. J., "The first order statistics of backscatter from the fractal branching vasculature," *J Acoust Soc Am* **146**(5), 3318–3326 (2019).
[25] Parker, K. J., "Shapes and distributions of soft tissue scatterers," *Phys Med Biol* **64**(17), 175022 (2019).
[26] Parker, K. J., Carroll-Nellenback, J. J., and Wood, R. W., "The 3D spatial autocorrelation of the branching fractal vasculature," *Acoustics* **1**(2), 369–381 (2019).
[27] Carroll-Nellenback, J. J., White, R. J., Wood, R. W., and Parker, K. J., "Liver backscatter and the hepatic vasculature's autocorrelation function," *Acoustics* **2**(1), 3–12 (2020).
[28] Parker, K. J. and Poul, S. S., "Burr, Lomax, Pareto, and logistic distributions from ultrasound speckle," *Ultrasonic Imaging* **42**(4-5), 203–212 (2020).
[29] Ge, G. R., Rolland, J. P., and Parker, K. J., "Speckle statistics of biological tissues in optical coherence tomography," *Biomedical Optics Express* **12**(7), 4179–4191 (2021).
[30] Niemczyk, M. and Iskander, D. R., "Statistical analysis of corneal OCT speckle: a non-parametric approach," *Biomedical Optics Express* **12**(10), 6407–6421 (2021).
[31] Rasmussen, M. K., Mestre, H., and Nedergaard, M., "Fluid transport in the brain," *Physiological Reviews* (2021).